Geomechanics and Engineering, *Vol. 24, No. 6 (2021) 573-588*
DOI: https://doi.org/10.12989/gae.2021.24.6.573

Hydro-mechanical coupling behaviors in the failure process of pre-cracked sandstone

Tingchun Li[1], Yiteng Du*[1], Qingwen Zhu[1], Yande Ren[2], Hao Zhang[1] and Jinlin Ran[1]

[1]*Shandong Key Laboratory of Civil Engineering Disaster Prevention and Mitigation, Shandong University of Science and Technology, Qingdao 266590, China*
[2]*Radiology Department, The Affiliated Hospital of Qingdao University, Qingdao 266590, China*

(Received September 9, 2020, Revised March 11, 2021, Accepted March 18, 2021)

Abstract. The interaction of cracks and water significantly affects the fracture mechanism of rocks. In this study, laboratory tests were conducted using sandstone samples containing a single fissure to explore the hydro-mechanical behaviors in the failure process of pre-cracked rocks. The internal crack characteristics were also analyzed using X-ray CT scanning. The results show that the confining pressure has the greatest effect on the mechanical properties (e.g., strengths, elastic modulus, and Poisson's ratio), followed by the fissure inclination and water pressure. At a lower fissure inclination, the confining pressure may control the type main cracks that form, and an increase in the water pressure increases the number of anti-wing cracks and the length of wing cracks and branch cracks. However, the fracture behaviors of samples with a higher fissure inclination are only slightly affected by the confining pressures and water pressures. The effect of fissure inclination on the internal crack area is reduced with the propagation from the fissure tips to the sample ends. The fissure inclination mainly affects the value of permeability but not affect the trend. The impact of pre-existing fissure on permeability is smaller than that of confining pressure and water pressure.

Keywords: sandstone; single fissure; experiment; mechanical properties; failure behavior; permeability

1. Introduction

Jointed rock mass widely exists in geotechnical engineering projects such as high slopes, tunnels, and underground excavations (Crider 2015, Son and Adedokun 2016, Bewick *et al*. 2019). The initiation and propagation of cracks have a significant effect on the strength, deformability and failure behaviors of rock mass (Li *et al*. 2015, Lee and Hong 2018, Hu *et al*. 2020). Furthermore, the interaction of cracks and water further reduce the stability of surrounding rocks (Maruvanchery and Kim 2018, Wang *et al*. 2019). Therefore, research on hydro-mechanical coupling behaviors in the failure process of pre-cracked rocks is very significant for controlling the stability of geotechnical engineering projects.

In the past decade, numerous efforts have been devoted to investigate the deformation and failure of pre-cracked rocks under anhydrous conditions. Different types of rock-like materials have been widely used in experimental study since the flaws are easy to fabricate. For example, Jin *et al*. 2017, Zhao *et al*. 2019 conducted uniaxial compression tests to investigate the failure process of rock-like samples containing a single flaw. Uniaxial compression tests on rock-like samples containing two (Tian and Yang 2017, Naderloo *et al*. 2019, Asadizadeh *et al*. 2019) or three flaws (Park and Bobet 2010, Xu and Li 2019) have been also symmetrically performed to investigate the effects of rock bridge parameters on the crack coalescence mechanism in pre-cracked rock-like materials. Moreover, Chen *et al*. 2019 experimentally investigated the crack initiation, propagation, and coalescence of gypsum samples containing multiple flaws. Similar pre-cracked cement mortar samples have been subjected to uniaxial compressive loads to study the influence of angle, spacing, flaw length, and rock bridge angle on the crack coalescence behaviors (Huang *et al*. 2019). Rock-like materials and real rocks have common characteristics for fracturing behaviors but also differences caused by the material properties (Lee and Jeon 2011). To investigate the fracturing mechanism of real rocks, Liu *et al*. (2020) experimentally studied the strain evolution of granite samples containing a single flaw. They found that the position of the strain concentration changed from within the flaw to the flaw tips with the increase in flaw angle. Wong and Xiong (2018) presented a method for multiscale interpretation of fracture behavior of single-flawed marble samples under uniaxial compression. Morgan *et al*. (2013) conducted uniaxial compression tests on granite samples with pre-existing flaw pairs. In their experimental results, crack coalescence trended from indirect to direct shear and combined shear-tensile to direct tensile coalescence as the flaw angle or rock bridge angle increased. Huang *et al*. (2016a), Wu *et al*. (2019) carried out triaxial compression tests on sandstone samples containing two flaws and found that the cracking behaviors depends not only on flaw geometry but also on confining pressure. In addition to laboratory tests, many numerical simulations using various methods such as DEM (Manouchehrian *et al*.

*Corresponding author, Ph.D.
E-mail: duyiteng2016@sdust.edu.cn

ISSN: 2005-307X (Print), 2092-6219 (Online)

Table 1 Summary of related publications

Condition	Method	Material	Flaw number	Load	Related publication
Anhydrous compression	Experiment	Rock-like	3	Uniaxial	Park and Bobet (2010)
			1		Jin *et al*. (2017)
			2		Tian and Yang (2017)
			1		Zhao *et al*. (2019)
			2		Naderloo *et al*. (2019)
			2		Asadizadeh *et al*. (2019)
			1/2/3		Xu and Li (2019)
			Multi		Chen *et al*. (2019)
			Multi		Huang *et al*. (2019)
			2		Lee and Jeon (2011)
		Real rock	2		
			2		Morgan *et al*. (2013)
			1		Wong and Xiong (2018)
			1		Liu *et al*. (2020)
			2	Triaxial	Huang *et al*. (2016)
			2		Wu *et al*. (2019)
	Numerical simulation	-	1	Uniaxial	Duriez *et al*. (2016)
			2		Fu *et al*. (2017)
			1/2		Pakzad *et al*. (2018)
			1		Mondal *et al*. (2019)
			2/3/4		Bastola and Cai 2019
			1	Biaxial	Manouchehrian *et al*. (2014)
			2	Triaxial	Huang *et al*. (2016)
Hydro-mechanical coupling compression	Experiment	Real rock	None	Triaxial+ water pressure	Heiland (2003)
					Alam *et al*. (2014)
					Xiao *et al*. (2020)
		Rock-like	4		Wang *et al*. (2020)
	Numerical simulation	-	None		Zeng *et al*. (2018)
					Yu *et al*. (2020)

2014, Duriez *et al*. 2016, Huang *et al*. 2016b, Bastola and Cai 2019), FLAC3D (Fu *et al*. 2017), ABAQUS (Pakzad *et al*. 2018), FEM (Mondal *et al*. 2019) have also been conducted to investigate the influence of flaw geometry, flaw number, and confining pressure on crack propagation and coalescence. These studies have contributed to better understanding the fracture mechanism of jointed rocks under anhydrous conditions.

In fact, the presence of water pressure affects the mechanical properties and fracture mechanism, making it different from rocks under anhydrous conditions. Thus, Heiland 2003 conducted triaxial seepage tests on sandstone to study the changes in hydraulic properties in the failure process of triaxial rock deformation. In their studies, the initial permeability was generally regained in the post-failure region. Additionally, the permeability increase showed a linear dependence on volumetric strain in the volumetric dilation stage. Alam *et al*. (2014) experimentally investigated the permeability evolution of tuff, sandstone, and granite under different confining pressures. They found that variations in rock type and confining pressure can cause obvious changes in rock permeability. Xiao *et al*. 2020 carried out triaxial compression tests on red sandstone under different seepage pressures. In their study, the variation laws of strength, deformation, and permeability during rock failure were symmetrically analyzed. Moreover, a piecewise functional relationship model between permeability and stress in the pre-peak failure process was established. Zeng *et al*. (2018) simulated the permeability behaviors of granite using the PFC2D and presented an improved flow-coupling algorithm to better reflect the preferential flow in rock fractures. Yu *et al*. (2020) calibrated the PFC2D mode particle stream through triaxial compression tests to investigate the strength and permeability characteristics of anisotropic sandstone. Furthermore, they also analyzed the synergistic effect between force chain distribution and failure patterns of anisotropic sandstone.

The related literature is summarized in Table 1. It can be seen that the previous studies of crack propagation and coalescence in pre-cracked rocks are mainly under anhydrous compressive conditions. Although Wang *et al*. 2020 experimentally studied the influence of hydraulic pressure on the strength, permeability and deformation properties of rock-like samples containing four identical pre-existing joints, the previous research on hydro-mechanical behaviors of rocks has been generally conducted on intact rock samples. However, experiments conducted on rock-like samples cannot fully reveal the hydro-mechanical behaviors of real rocks. The strength and deformation characteristics of real jointed rocks under the interaction between crack propagation and water seepage have not been completely revealed.

Therefore, our recent work (Du *et al*. 2020) experimentally investigated the effects of rock bridge parameters on the hydro-mechanical properties of sandstone containing two fissures with constant geometric properties. Nonetheless, due to the interaction of the two fissures, it is difficult to reveal the crack initiation strength, crack propagation, and permeability characteristic induced by each fissure. And the true roles of each fissure in the deformation failure mechanisms in the process of crack coalescence cannot adequately explained. It is also necessary to systematically investigate the influence of single-fissure properties on the fracture mechanism and permeability evolution of pre-cracked rocks. Therefore, the present research conducted a series of hydro-mechanical coupling tests on sandstone samples containing a single fissure with different inclinations. The main aims focus on the following: (1) systematically investigating the influence of fissure inclination on strength and deformation properties in the failure process of single-fissure rocks under different confining pressures and water pressures; (2) comparing the fracture patterns with the change in fissure inclination under the coupling of various confining pressures and hydraulic

Table 2 Physical and mechanical properties of the tested sandstone

Properties	Density (kg/m^3)	Initial porosity (%)	Initial permeability (m^2)	Tensile strength (MPa)	UCS (MPa)	Elastic modulus (GPa)	Poisson's ratio
Value	2392	7.55	10^{-18}-10^{-17}	4.78	73.07	22.35	0.31

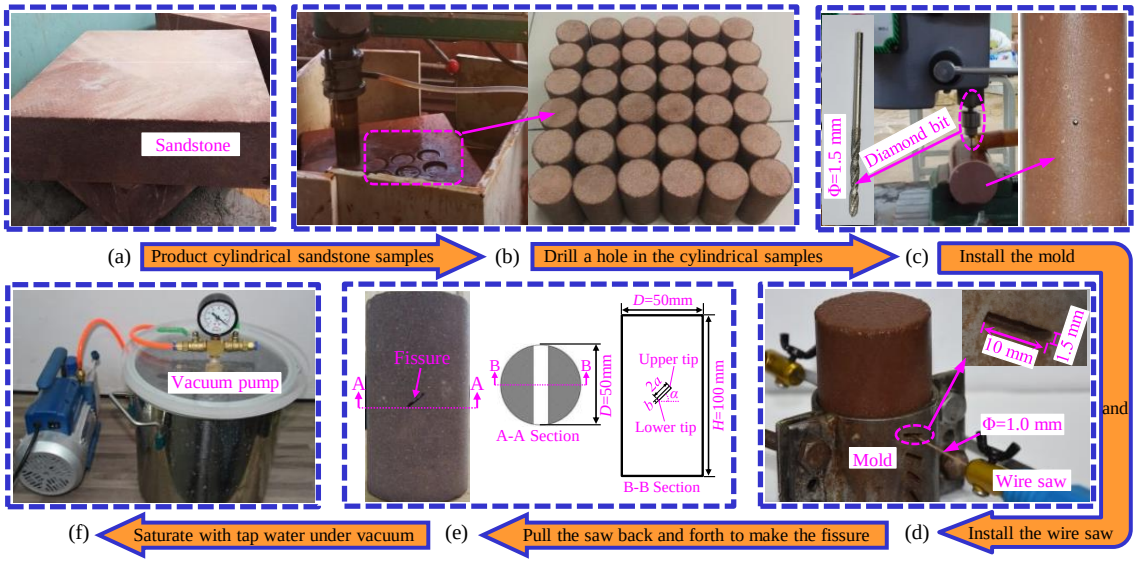

Fig. 1 Preparation of the tested samples

Table 3 Symbols of the influence factors

Symbols	Influence factors	Units	Values
'*I*'	Intact sample	-	-
'α'	Fissure inclination	°	15/30/45/60/75
'P_c'	Confining pressure	MPa	5/10/15
'P_w'	Water pressure	MPa	2/5/8

pressures; (3) quantitatively analyzing the effect of fissure inclination on internal crack characteristics based on CT images; (4) discussing the permeability evolution in volumetric deformation stages of intact sandstones and single-fissure sandstones in detail.

2. Experimental material and procedure

2.1 Sandstone material and preparation of samples

In this research, the tested rock material was red sandstone, which was collected from Tai'an city in the Shandong province of China. The sandstone is composed mainly of feldspar (74.2%), quartz (13.0%) and montmorillonite (12.8%) according to X-ray diffractometer (XRD) analysis. According to the laboratory testing analysis, the physical and mechanical properties of the sandstone were obtained, as shown in Table 2. Fig. 1 shows the preparation method of intact samples and single-fissure samples. To reduce the dispersion, all tested rock samples were drilled in an adjacent position of the same rock block without any macroscopic cracks. The tested samples were machined into a cylindrical shape with a height of 100 mm and a diameter of 50 mm. Both ends of these rock samples were carefully polished to produce flat parallel surfaces and the error of unevenness was less than 0.1 mm. Then, a penetration-type fissure with a length of 10 mm and a width of 1.5 mm was prepared on the samples. Afterward, the tested samples were saturated with tap water under vacuum before mounting in the triaxial cell.

To investigate the influence of the fissure inclination, confining pressure, and water pressure on the strength, deformation, fracture pattern, and permeability evolution of single-fissure rocks, 5 inclinations, 3 confining pressures, and 3 water pressures were designed in this study. In the following parts of the paper, some symbols are used to denote these influence factors, as shown in Table 3. Furthermore, the tested samples are named using by the combinations of these symbols. For example, '*I*-P_c5-P_w2' denotes the intact sample under 5 MPa confining pressure coupled with 2 MPa water pressure, and 'α15°-P_c15-P_w8' denotes the sample containing a single fissure with 15° inclination under 15 MPa confining pressure coupled with 8 MPa water pressure.

2.2 Testing equipment and procedure

All hydro-mechanical coupling tests were performed in

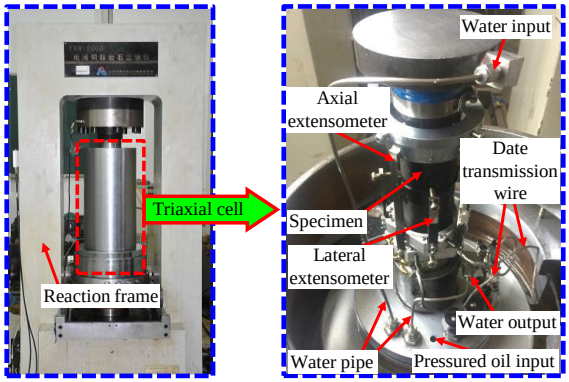

Fig. 2 TAW-2000 electrohydraulic servo-controlled testing equipment

a TAW-2000 electrohydraulic servo-controlled testing machine, as shown in Fig. 2. The maximum axial loading, confining pressure, and water pressure of this testing equipment were 2000 kN, 100 MPa, and 60 MPa, respectively. Before the tests, the sample was circumferentially wrapped in a shrinkable plastic sleeve to separate the confining pressure from the water pressure and mounted with both axial and lateral extensometers to collect deformation data. The measurement capacity and reading accuracy of the extensometers are 0-4 mm and ±1%, respectively. After the assembled sample was placed into the triaxial cell, the confining pressure induced by hydraulic oil was gradually increased to the required value and then kept constant throughout the experiment. When the hydrostatic stress state, which was a stable state, was reached, the inlet water pressure at the upstream end of the sample was gradually applied to a predetermined value, and the outlet was open to the atmosphere. The outlet volumetric water flow rate at the downstream end of the sample was measured in real time by a water flow meter on the testing system. When the flow rate reached a constant value, the axial stress was increased under constant axial displacement control at a rate of 0.02 mm/min until the end of the test.

The steady-state flow tests are more suitable to obtain the permeability of rocks when the permeability $k \geq 10^{-19}$ m^2 (Davy *et al*. 2007, Chen *et al*. 2017a). The initial permeability of the tested sandstone is estimated to be on the order of 10^{-18}~10^{-17} m^2. Therefore, the steady-state flow method is chosen in this study. Darcy's law is usually assumed to be valid for steady-state flow permeability tests. Based on Darcy's law and the measured water flow rate, the permeability of the sample with a pre-existing fissure can be calculated as follows (Xiao *et al*. 2020):

$$k = \frac{Q\mu_f H}{\Delta p A} \quad (1)$$

where k is the permeability (m^2); Q is the water flow rate (m^3/s); μ_f is the dynamic viscosity of water, where the μ_f value at room temperature is 1.005×10^{-3} Pa·s; H is the length of the sample (m); ΔP is the water pressure difference applied between both end planes of the rock sample (Pa); and A is the cross-sectional area of the sample (m^2).

3. Mechanical properties

3.1 Stress-strain curves

To investigate the mechanical characteristics of single-fissure sandstone, the influence of heterogeneity on the stress-strain curves of tested samples is first discussed. A random group of single-fissure samples with the same inclination (α=45°) are selected to conduct the repeated tests under confining pressure of 15 MPa and water pressure of 2 MPa. The stress-strain curves of single-fissure samples in the repeated tests are shown in Fig. 3. These stress-strain curves have very good consistency, and the coefficient of variation on peak strength is 1.41%. It can be seen that the heterogeneity has little effects on the mechanical properties of the samples with the same inclination under a constant confining pressure coupled with a constant water pressure. Therefore, the experimental results in this study can be used to discuss the effects of inclination, confining pressure, and water pressure on hydro-mechanical behaviors on the single-fissure sandstones.

3.1.1 Effect of confining pressure on stress-strain curves of single-fissure samples

The stress-strain curves of intact samples and single-fissure samples under various confining pressures (5, 10, and 15 MPa) coupled with a constant water pressure (2 MPa) are shown in Fig. 4. The stress-strain curves show a similar shape, regardless of the fissure. In the pre-peak stage, the slopes of the curves all increase with an increase in confining pressure, especially near the peak point. In the post-peak stage, the stress decrease rate of the single-fissure samples is greater than that of the intact samples especially under a lower confining pressure. This indicates that the brittle failure characteristics of sandstone are more remarkable with the existence of the fissure.

3.1.2 Effect of water pressure on stress-strain curves of single-fissure samples

The stress-strain curves of intact samples and single-fissure samples under a constant confining pressure (15 MPa) coupled with various water pressures (2, 5, and 8 MPa) are shown in Fig. 5.

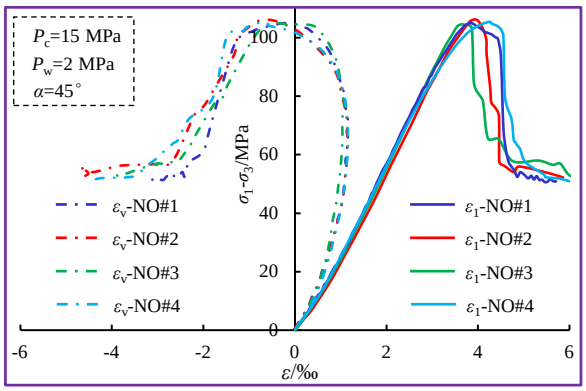

Fig. 3 Typical effect of heterogeneity on stress-strain curves of sandstone samples containing a single fissure (α=45°) under hydro-mechanical coupling conditions (P_c=15 MPa and P_w=2 MPa)

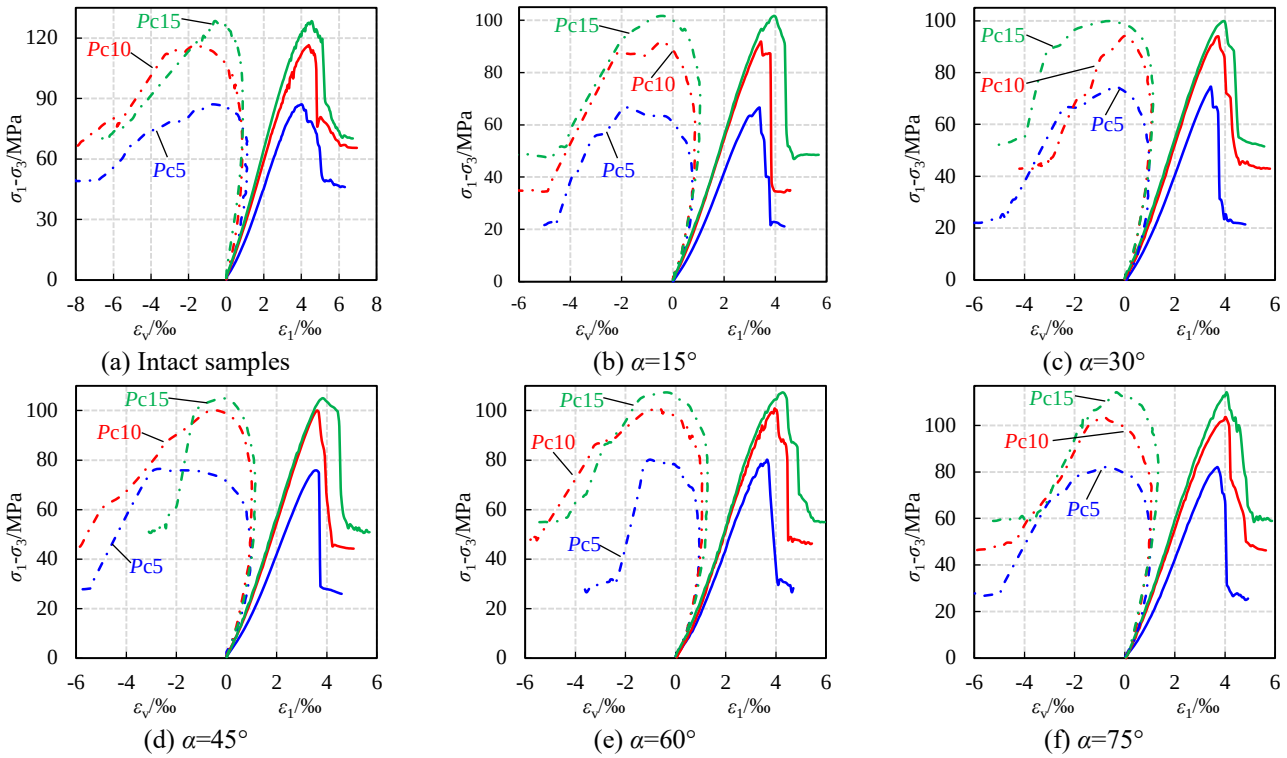

Fig. 4 Stress-strain curves of tested samples under different confining pressures

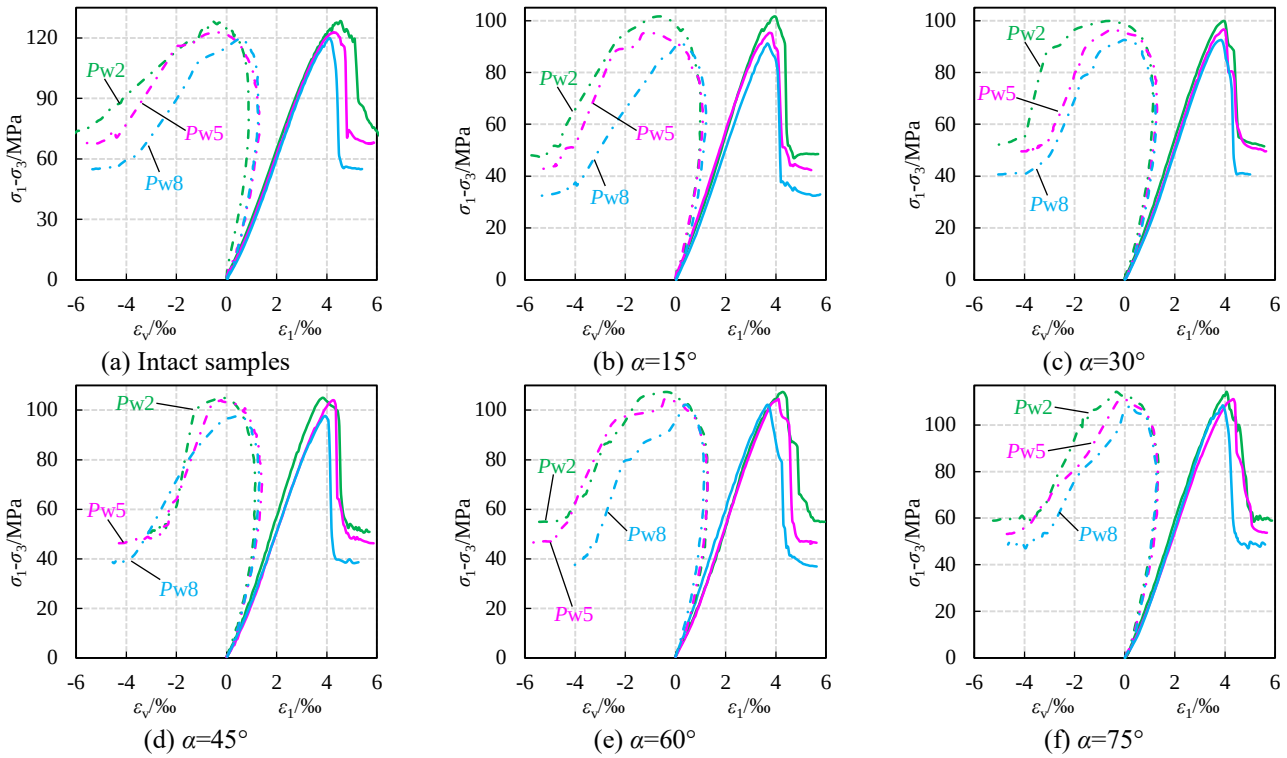

Fig. 5 Stress-strain curves of tested samples under different water pressures

In Fig. 5, the strength parameters and the slope of stress-strain curves of intact samples and single-fissure samples all decrease with the increase in the water pressure. The stress decrease rate in the post-peak stage of the curves is positively correlated with the water pressure, especially with a lower inclination ($\alpha \leq 45°$).

3.2 Strength properties in complete stress-strain process

The crack initiation threshold σ_{ci}, crack damage threshold σ_{cd}, and peak strength σ_c are three important stress thresholds related to the rock failures in the complete stress-

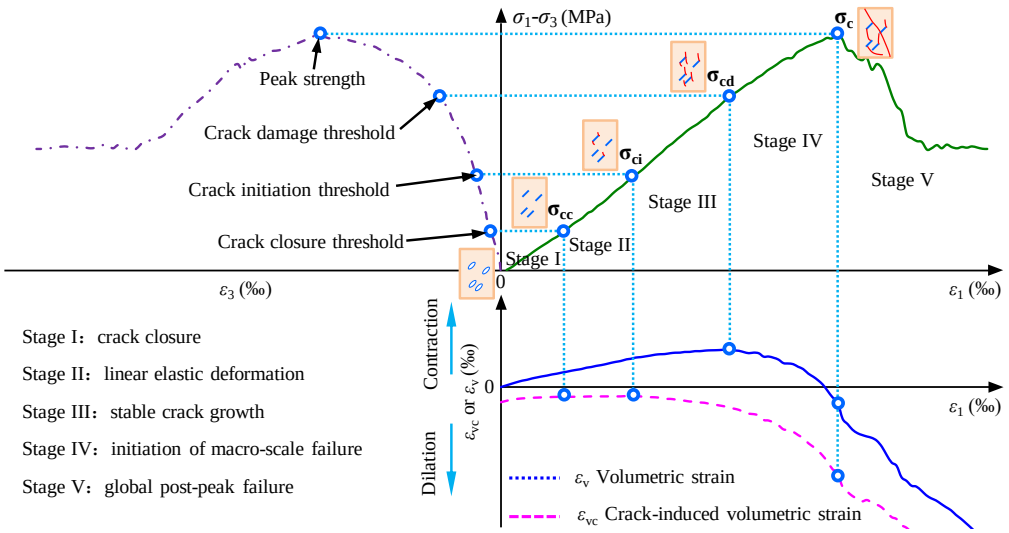

Fig. 6 Crack stress threshold points in the complete stress-strain process (modified from Martin and Chandler 1994, Chen *et al*. 2017b, Bruning *et al*. 2018)

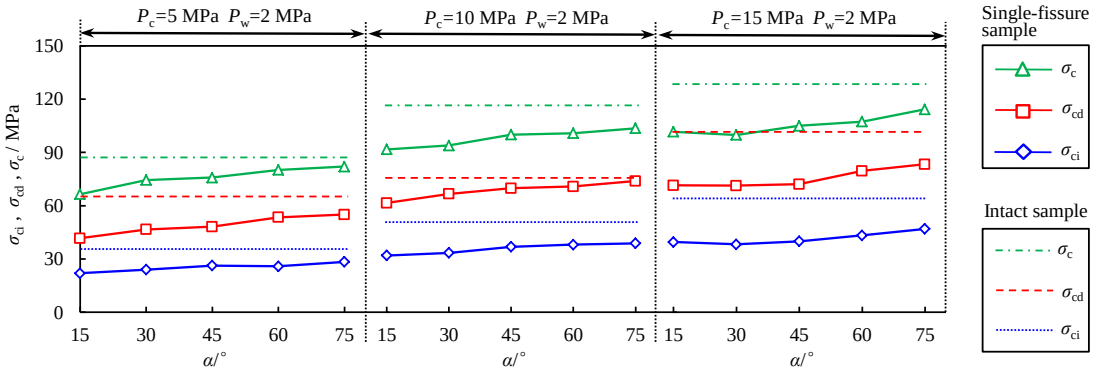

Fig. 7 Values of σ_{ci}, σ_{cd}, and σ_c of the tested samples under different confining pressures

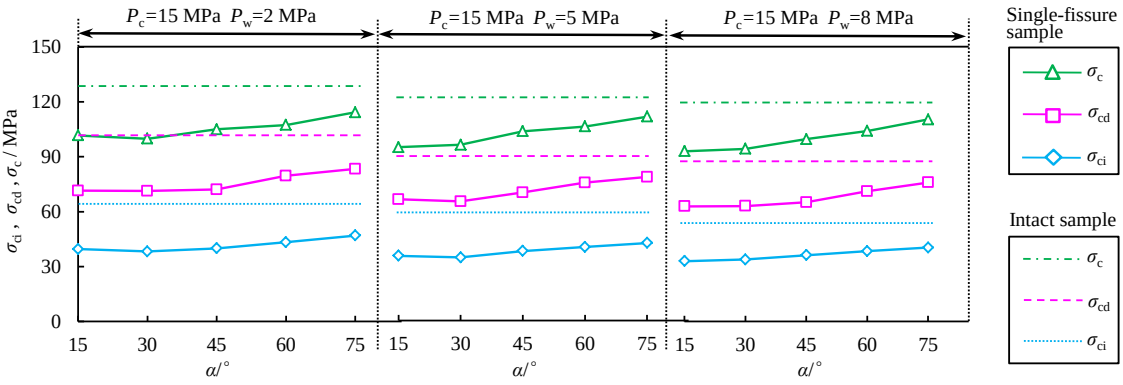

Fig. 8 Values of σ_{ci}, σ_{cd}, and σ_c of the tested samples under different water pressures

strain process (Martin and Chandler 1994, Chen *et al*. 2017b, Bruning *et al*. 2018), as shown in Fig.6.

The value of σ_{ci} corresponds to the axial stress at the inflection of the stress-strain curve from the crack-induced volumetric strain ε_{vc} to the axial strain ε_1 and it is the stress at the beginning of stable crack growth. Additionally, σ_{cd} corresponds to the stress where the volumetric strain becomes decreasing, and it is the stress for the beginning of unstable crack propagation. The values of ε_{vc} and ε_v can be calculated as follows (Chen *et al*. 2017b):

$$\begin{cases} \varepsilon_{vc} = \varepsilon_v - \dfrac{1-2\mu}{E}(\sigma_1 + 2\sigma_3) \\ \varepsilon_v = \varepsilon_1 + 2\varepsilon_3 \end{cases} \tag{2}$$

where μ denotes the Poisson's ratio; E denotes the elastic modulus; σ_1 denotes the axial stress; σ_3 denotes the confining pressure; ε_1 denotes the axial strain; and ε_3 denotes the lateral strain.

Table 4 Elastic modulus and Poisson's ratio of tested samples

	Elastic modulus (GPa)						Poisson's ratio					
	I	*F*15	*F*30	*F*45	*F*60	*F*75	*I*	*F*15	*F*30	*F*45	*F*60	*F*75
P_c5 P_w2	28.06	24.95	25.69	25.59	27.73	28.29	0.240	0.272	0.241	0.246	0.251	0.248
P_c10 P_w2	31.33	30.36	30.31	30.04	30.90	31.42	0.288	0.253	0.237	0.271	0.235	0.254
P_c15 P_w2	33.66	31.72	30.61	32.31	32.22	33.26	0.296	0.232	0.255	0.263	0.202	0.201
P_c15 P_w5	35.01	29.65	30.13	29.89	31.06	31.93	0.226	0.212	0.206	0.199	0.205	0.203
P_c15 P_w8	34.72	28.95	29.86	29.18	30.72	31.54	0.204	0.202	0.209	0.201	0.207	0.204

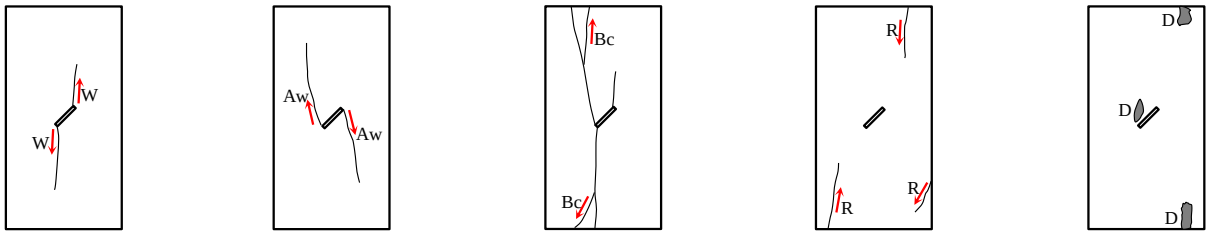

Wing crack Anti-wing crack Branch crack Remote crack Detached block

Fig. 9 Different types of cracks on single-fissure samples under hydro-mechanical coupling condition

3.2.1 Strength properties of single-fissure samples under different confining pressures

The values of σ_{ci}, σ_{cd}, and σ_c of single-fissure samples under a constant water pressure coupled with different confining pressures are illustrated in Fig. 7. Compared to intact samples, the values of σ_{ci}, σ_{cd}, and σ_c of single-fissure samples under various confining pressures (5-15 MPa) decrease by at most 40.0%, 35.8%, and 23.6%, respectively. Moreover, the values of σ_{ci}, σ_{cd}, and σ_c of single-fissure samples decrease by at most 44.38%, 41.62%, and 34.53%, respectively, due to a decrease in the confining pressure from 15 to 5 MPa. The fissure inclinations corresponding to the largest reductions in the values of σ_{ci}, σ_{cd}, and σ_c are always 15°. It can be concluded that the crack initiation threshold, crack damage threshold, and peak strength of sandstone are weakened greatly by the existence of the fissure and the decrease of the confining pressure. When the fissure inclination is lower than 45°, the effects of the fissure and confining pressure are more remarkable.

3.2.2 Strength properties of single-fissure samples under different water pressures

The values of σ_{ci}, σ_{cd}, and σ_c in the complete stress-strain process of single-fissure samples under a constant confining pressure coupled with different water pressures are illustrated in Fig. 8. Compared to intact samples, the values of σ_{ci}, σ_{cd}, and σ_c of single-fissure samples under various water pressures (2-8 MPa) decrease by at most 41.9%, 29.6%, and 23.9%, respectively. The fissure inclinations associated with the maximum decreases are all lower than 45°. Furthermore, due to an increase in water pressure from 2 to 8 MPa, the values of σ_{ci}, σ_{cd}, and σ_c of single-fissure samples decrease by at most 16.5%, 12.0%, and 10.3%, respectively. The corresponding inclinations are always 15°. It can be concluded that the strength properties of sandstone samples exhibit a significant reduction caused by the interaction of water pressure and pre-existing fissure, especially with a lower fissure inclination ($\alpha \leq 45°$).

3.3 Elastic modulus and Poisson's ratio

Table 4 shows the elastic modulus E and Poisson's ratio μ of intact samples and single-fissure samples under different confining pressures and water pressures.

3.3.1 Effect of confining pressure on elastic modulus and Poisson's ratio

Compared to intact samples, the elastic moduli of single-fissure samples under P_c= 5, 10, and 15 MPa decrease by at most 11.1%, 4.1%, and 9.1%, respectively. The weakening effects of the fissure with a lower inclination ($\alpha \leq 45°$) on the elastic moduli are more significant than those with a higher inclination ($\alpha > 45°$). Furthermore, the elastic moduli of single-fissure samples all decrease with a decrease in confining pressure. The fissure inclination corresponding to the largest reduction in elastic modulus is 45°. When P_c= 5 MPa, the effect of the fissure on Poisson's ratio is small. Compared to intact samples, Poisson's ratio of single-fissure samples under P_c=10 and 15 MPa decrease by at most 18.4% and 32.1%, respectively. Additionally, the effects of the single fissure on Poisson's ratio are more remarkable when $\alpha > 45°$.

3.3.2 Effect of water pressure on elastic modulus and Poisson's ratio

Compared to intact samples, the elastic moduli of single-fissure samples under P_w=2, 5, and 8 MPa decrease by at most 9.1%, 15.3%, and 16.6%, respectively. The elastic moduli of single-fissure samples are negatively correlated with water pressure. When α=45°, the weakening

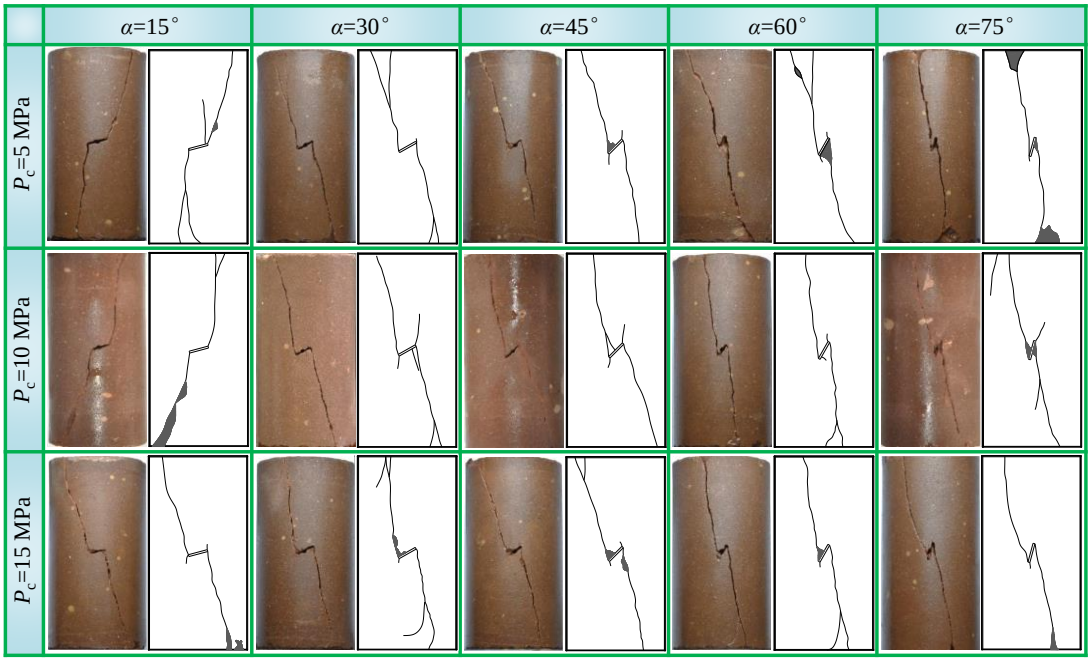

Fig. 10 Failure of single-fissure specimens under different confining pressures

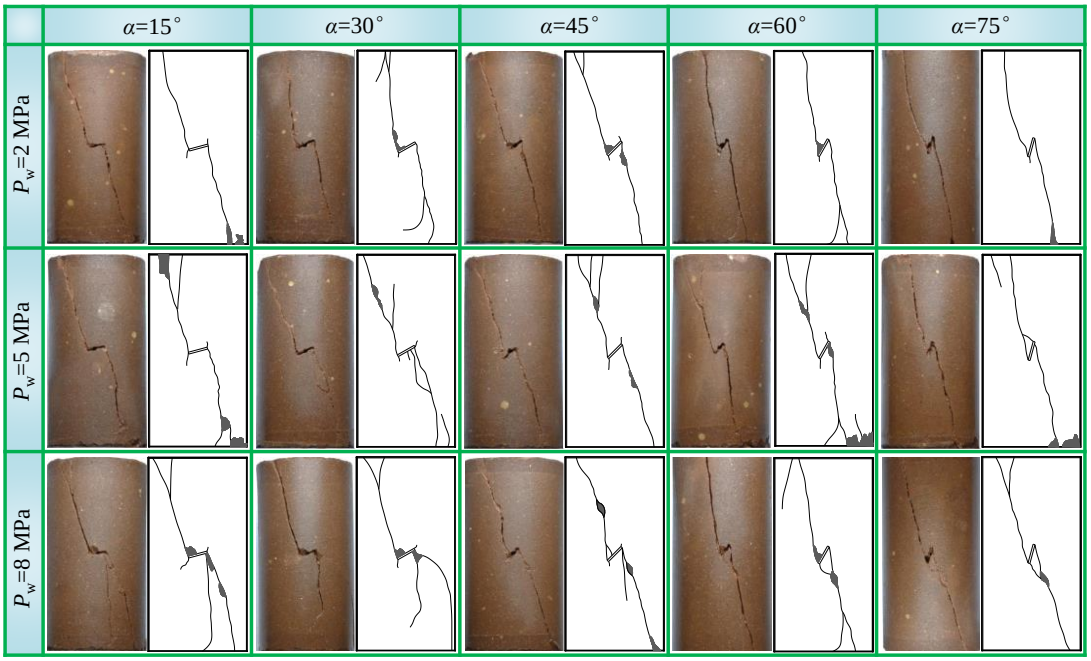

Fig. 11 Failure of single-fissure specimens under different water pressures

effect of water pressure on the elastic moduli of single-fissure samples is most significant. Furthermore, the influence of the fissure on Poisson's ratio of sandstone samples under a higher water pressure (5 or 8 MPa) is slight. The influence of water pressure on Poisson's ratio also changes with fissure inclinations.

4. Failure behaviors

4.1 Surface failure modes

Fig. 9 illustrates the different types of cracks on single-fissure samples under the hydro-mechanical coupling condition. In Fig. 9, "W" denotes the wing cracks, which initiate at the tips of the fissure and propagate to the two ends of the samples; "Aw" denotes the anti-wing cracks, which also initiates from the fissure tips but whose propagation direction is opposite to the wing cracks; "Bc" denotes the branch crack, which generate on the wing cracks and anti-wing cracks; "R" denotes the remote crack, which is separated from the other cracks; and "D" denotes the detached block.

4.1.1 Effect of confining pressure on failure mode of single-fissure samples

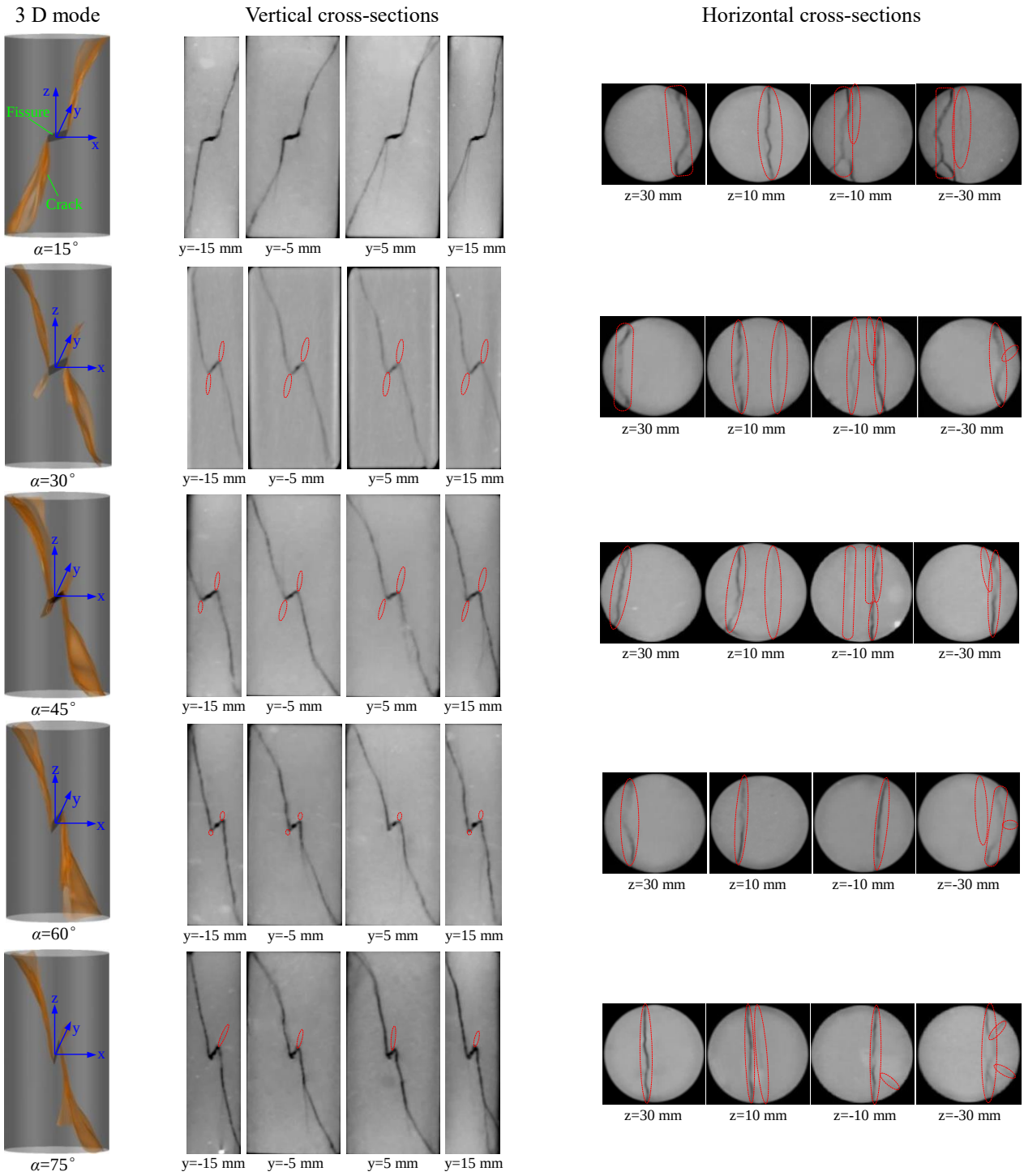

Fig. 12 CT images of singe-fissure samples

Fig. 10 shows the ultimate failure modes of single-fissure samples under different confining pressures (P_c=5, 10, and 15 MPa) coupled with a constant water pressure (P_w= 2 MPa). When P_c=5 MPa, P_w= 2 MPa, and α=15°, the failure of single-fissure sample is caused mainly by three wing cracks generated at the two tips of the pre-existing fissure. Additionally, a shear branch crack and a detached block following the expansion of the left and right wing cracks. When P_c=10 MPa, the failure mode changes only slight: the number of wing cracks decreases from 3 to 2. When P_c=15 MPa, the failure is mainly caused by two shear anti-wing cracks generated at the two tips of the pre-existing fissure. Additionally, the lengths of wing cracks are less than 20% of the pre-existing fissure.

In addition, the failure of the tested samples at the fissure inclinations of 30-75° under different confining pressures (P_c=5, 10, and 15 MPa) coupled with a containing water pressure (P_w=2 MPa) is caused mainly by shear or tensile-shear composite anti-wing cracks that propagate through the bottom and the top boundaries of the sample.

Table 5 Effect of fissure inclination on the internal crack area in horizontal cross-sections

Horizontal cross-sections	Internal crack area (mm^2)				
	α=15°	α=30°	α=45°	α=60°	α=75°
z=30 mm	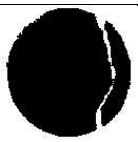 78.92 mm^2	 75.94 mm^2	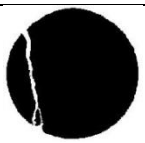 50.56 mm^2	 68.93 mm^2	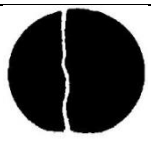 53.02 mm^2
z=10 mm	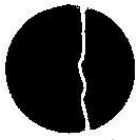 77.66 mm^2	 129.54 mm^2	 114.44 mm^2	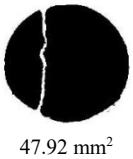 47.92 mm^2	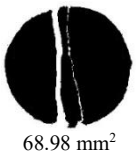 68.98 mm^2
z=-10 mm	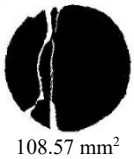 108.57 mm^2	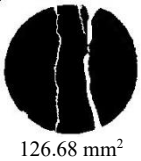 126.68 mm^2	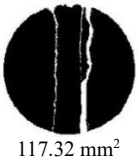 117.32 mm^2	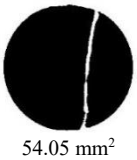 54.05 mm^2	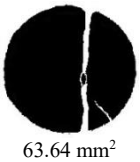 63.64 mm^2
z=-30 mm	 136.91 mm^2	 72.13 mm^2	 66.97 mm^2	 92.65 mm^2	 103.62 mm^2

Additionally, one or two short wing cracks whose lengths are shorter than the pre-existing fissure are accompanied. The propagation direction of the anti-wing cracks is closer to the axial loading direction, due to an increase in inclination and a decrease in confining pressure. In addition, the length and the number of wing cracks are all negatively correlated with the confining pressure.

4.1.2 Effect of water pressure on failure mode of single-fissure samples

Fig. 11 shows the ultimate failure modes of single-fissure samples under a constant confining pressure (P_c=15 MPa) coupled with different water pressures (P_w= 2, 5, and 8 MPa). The failures of samples under P_c=15 MPa and P_w= 2 MPa are analyzed in section 4.1.1.

When P_c=15 MPa and P_w= 5 MPa, the propagation paths of anti-wing cracks are similar to those under P_c=15 MPa and P_w=2 MPa. However, there are remarkable increases in the length and the number of wing cracks and branch cracks. Interestingly, when the fissure inclination is 30°, a short tensile anti-wing crack is generated near the upper tip of the pre-existing fissure, and it converges on the right shear anti-wing crack in the propagation process. Furthermore, when the fissure inclination is 75°, a shear wing crack is generated from the right tip of the pre-existing fissure, and it converges on the left shear anti-wing crack after propagating approximately 80% of the length of the pre-existing fissure.

When P_c=15 MPa and P_w= 8 MPa, the failures of the samples with a lower inclination ($\alpha \leq 45°$) are caused mainly by the propagations of two shear anti-wing cracks and a tensile anti-wing crack. In addition, the lengths and opening widths of the tensile anti-wing cracks decrease with an increase in the inclination. The failures of the samples with a higher inclination (α>45°) are caused mainly by two shear anti-wing cracks. Furthermore, a shear wing crack initiates from the left tip of the pre-existing fissure and converges on the right shear anti-wing crack, where a detached block is generated.

It can be concluded that the increase in water pressure promotes the initiation and growth of cracks, especially anti-wing cracks and branch cracks. In addition, the failure around the pre-existing fissure of the samples under a greater water pressure is more serious, especially with a higher inclination.

4.2 Inner failure behavior

X-ray CT scanning is performed on single-fissure samples after coupled hydro-mechanical triaxial compressive failure to analyze the internal crack behaviors. Taking the samples under a confining pressure of 10 MPa coupled with a water pressure of 2 MPa as examples, the three-dimensional images, vertical and horizontal cross-sections of the samples are shown in Fig. 12.

In Fig. 12, the primary cracks leading to the internal failure of single-fissure samples are anti-wing cracks, except for α=15°. The propagation path of the primary cracks changes along both the height (Z) and the diameter (Y). In the process by which the primary cracks propagated from the fissure tips to the top and bottom ends, the shapes of the primary cracks gradually transform into a curved surface, especially when α<45°. Moreover, the farther the distance away from the surface of the samples, the more remarkable the changes in primary crack propagation paths. The crack propagation angle (the angles between the crack propagation direction and the axial loading direction) generally increases in the cracking process from the tips of

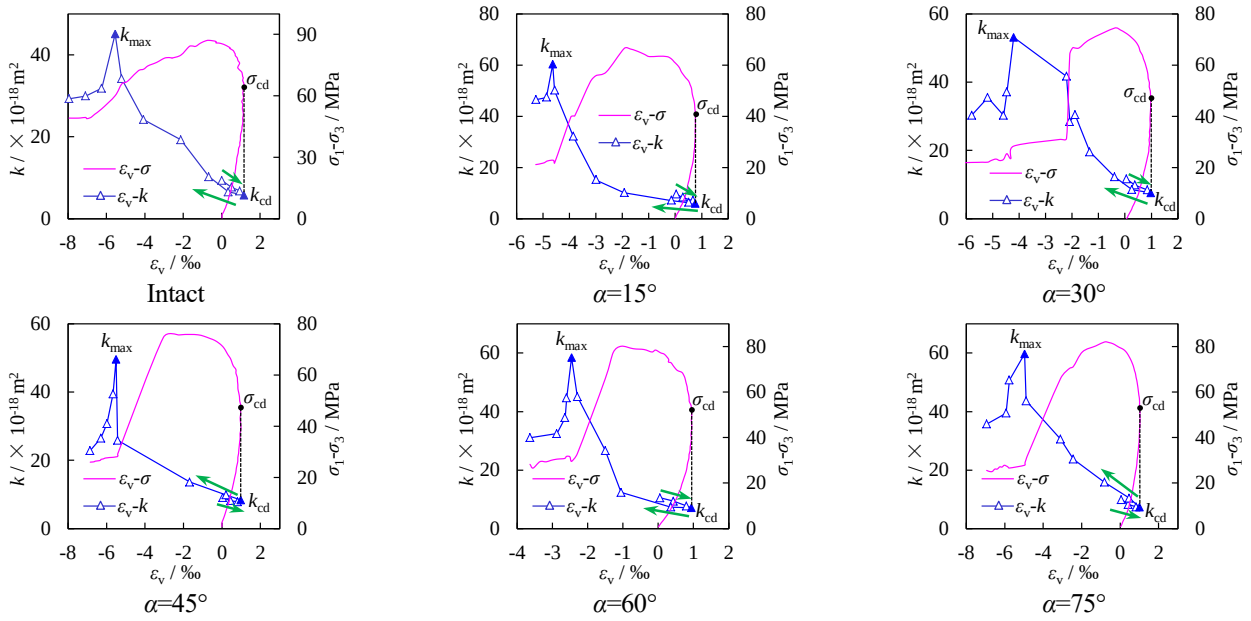

Fig. 13 Permeability-volumetric strain curves (P_c=5 MPa P_w=2 MPa)

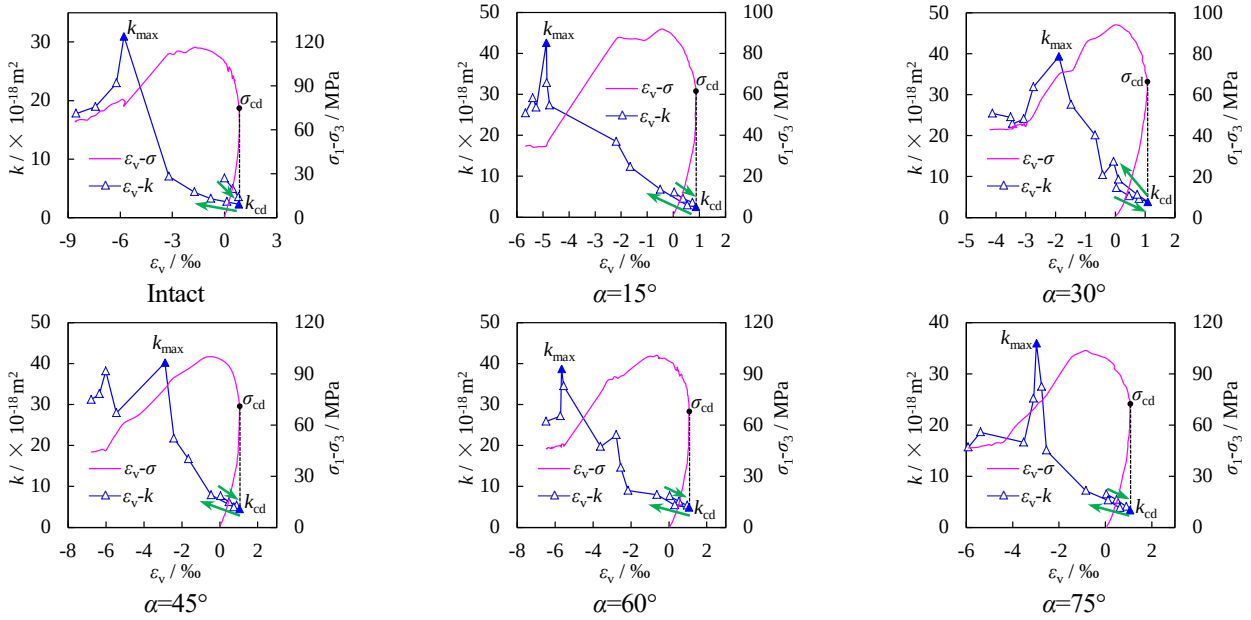

Fig. 14 Permeability-volumetric strain curves (Pc=10 MPa Pw=2 MPa)

the fissure to the ends of samples. Different from the primary cracks, the branch cracks are generally generated near the surface of samples and do not penetrate the horizontal cross-sections.

The horizontal CT images were processed using Matlab software (Yang *et al*. 2015) and changed to binarized pictures, as shown in Table 5. The white regions represent the cracks, whereas the black regions represent intact rocks. The ratio of white to total pixels of the horizontal cross-section is the proportion of the crack area. It can be seen that the internal damage area also changes with the fissure inclination. When z=30 mm and z=-30 mm, the maximum values of the crack area in horizontal cross-sections both occur at α=15°. As the inclination transforms from 15° to 75°, the greatest variations of the crack area in horizontal cross-sections, corresponding to z=30 mm and z=-30 mm, are 28.36 and 69.94 mm^2, respectively. When z=10 mm and z=-10 mm, the maximum values of the crack area in horizontal cross-sections both occur at α=30°. With the changes in inclinations (15-75°), the greatest variations of the crack area in horizontal cross-sections, corresponding to z=10 mm and z=-10 mm, are 81.62 and 72.63 mm^2, respectively. Therefore, the influence of fissure inclinations on the internal damage area near the fissure tips is more significant than that near the ends of samples under hydro-mechanical coupling conditions.

5. Permeability behaviors

5.1 Effects of confining pressures on permeability evolution of single-fissure samples

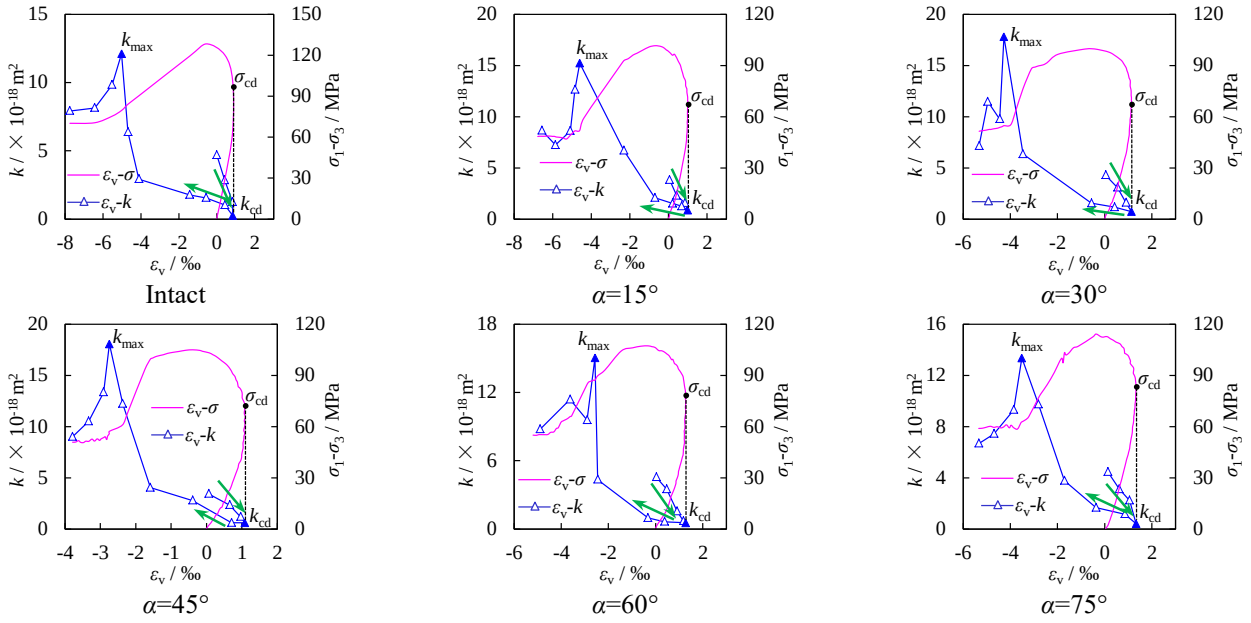

Fig. 15 Permeability-volumetric strain curves (Pc=15 MPa Pw=2 MPa)

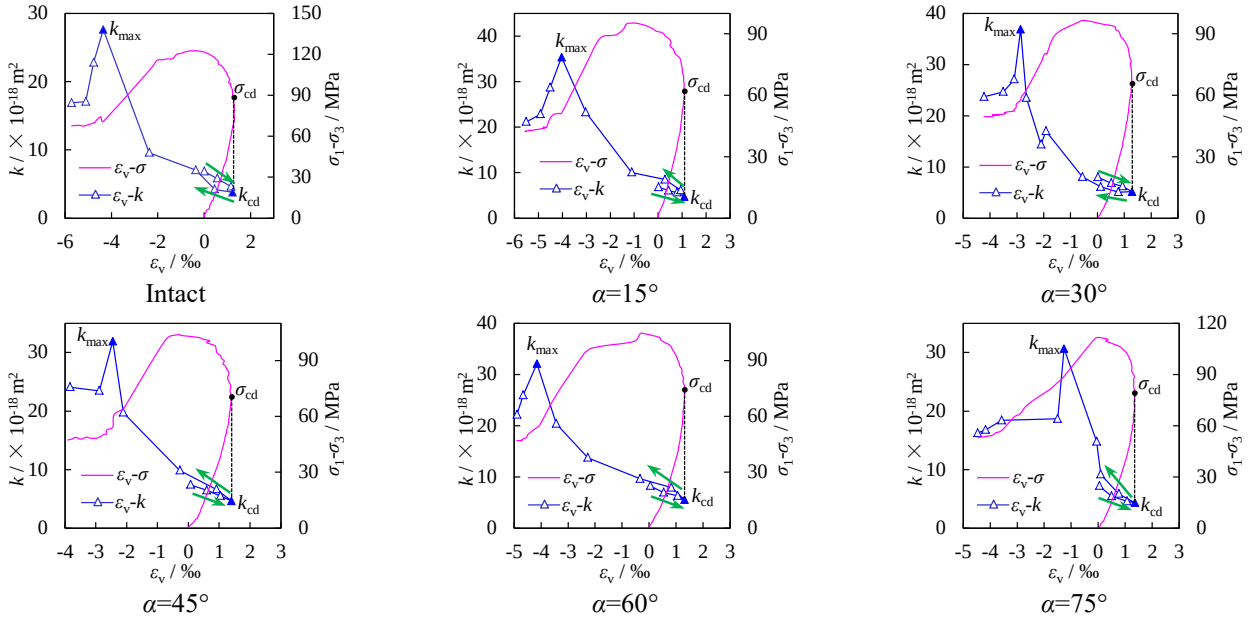

Fig. 16 Permeability-volumetric strain curves (P_c=15 MPa P_w=5 MPa)

The permeability-volumetric strain (k-ε_v) curves of the tested sandstone under different P_c coupled with a constant P_w are shown in Figs. 13-15. k_{cd} is the permeability corresponding to the inflection point of crack damage threshold σ_{cd}, at this inflection point, the volumetric strain changes from increasing to decreasing. k_{max} is the maximum permeability on the permeability-volumetric strain curves of sandstone samples.

In the volumetric contraction stage (σ_1-σ_3 < σ_{cd}), the permeability values of both intact samples and single-fissure samples first decrease and then increase with a slow rate. The turning point value of volumetric strain is positively correlated with confining pressure, especially when α>45°. Some of these curves at the turning point transforms from downward bending to upward bending with a decrease in confining pressure. In the volumetric dilation stage (after reaching σ_{cd}), the permeability increases at a fast rate caused by crack propagation and coalescence. k_{cd} and k_{max} of intact sample decease by 5.5×10^{-18} and 33.0×10^{-18} m^2, respectively, due to the increase in confining pressure from 5 MPa to 15 MPa. Additionally, the largest reductions in k_{cd} and k_{max} of single-fissure samples induced by the corresponding increases in confining pressures are 7.8×10^{-18} and 46.4×10^{-18} m^2, respectively. In addition, the fissure inclination does not affect the permeability trend, but affects the value. Compared to intact samples, the k_{cd} and k_{max} of single-fissure samples increase by at most 2.6×10^{-18} and 18.3×10^{-18} m^2, respectively, under confining pressure of 5 MPa coupled with water pressure of 2 MPa. The influence of the fissure on permeability values

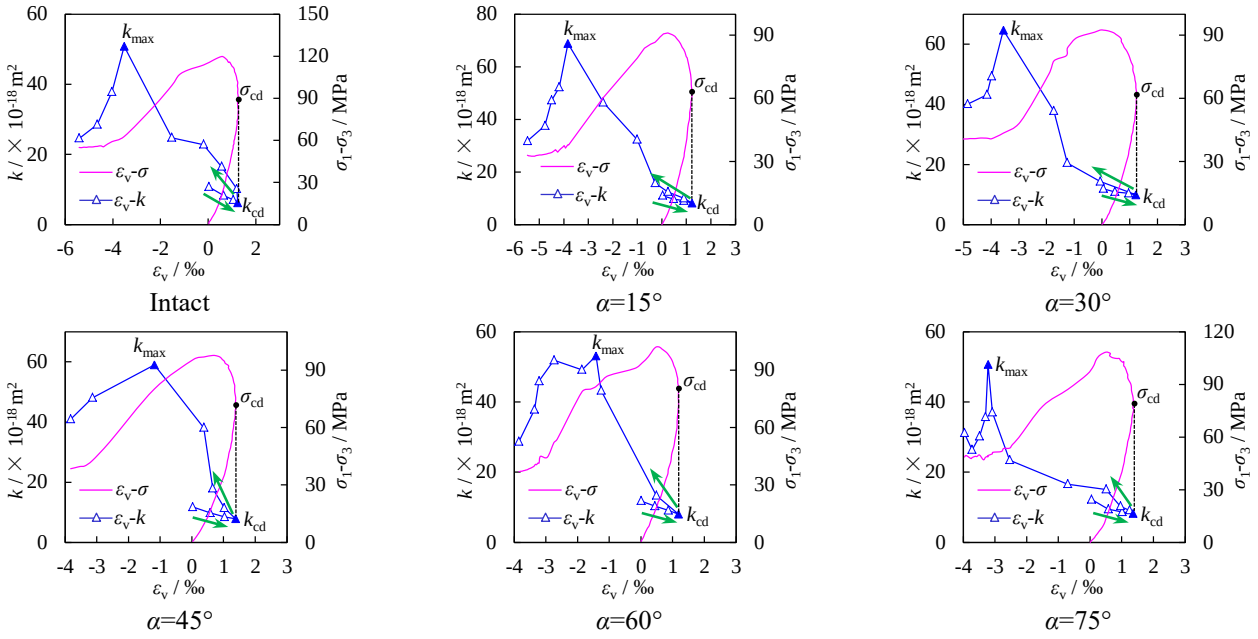

Fig. 17 Permeability-volumetric strain curves (P_c=15 MPa P_w=8 MPa)

decreases with increasing confining pressure. In addition, the changes in k_{max} induced by fissure inclination are more remarkable than those of k_{cd}, especially under a lower confining pressure.

5.2 Effects of water pressures on permeability evolution of single-fissure samples

The permeability-volumetric strain curves of the tested sandstone under P_c=15 MPa coupled with P_w=5 MPa and 8 MPa are shown in Figs. 16 and 17. With an increase in water pressure, the permeability curves at the turning point (k_{cd}) in the contraction stage transform from a downward bending shape to an upward bending shape. k_{cd} and k_{max} of the intact sample increase by 6.0×10^{-18} and 38.7×10^{-18} m^2, respectively, due to the increase in water pressure from 2 MPa to 8 MPa. Furthermore, the largest improvements in k_{cd} and k_{max} of single-fissure samples induced by the corresponding increases in water pressures are 9.1×10^{-18} and 53.6×10^{-18} m^2. Compared to intact samples, k_{cd} and k_{max} of single-fissure samples increase by at most 3.7×10^{-18} and 21.0×10^{-18} m^2 under P_c=15 MPa coupled with P_w=8 MPa. The improvement in permeability induced by the single fissure is positively correlated with the water pressure. Moreover, the greater the water pressure, the more remarkable the influence of fissure inclination on the permeability.

6. Discussion

6.1 Comparison with previous studies

Table 1 shows that the previous studies of fracture behaviors on pre-cracked rock and rock-like samples are always performed under anhydrous compressive conditions. Unlike the previous studies, the effects of water pressure and confining pressure on the mechanical properties (see Figs. 7 and 8) and fracture patterns (see Figs. 10 and 11) of single-fissure sandstone were systematically investigated in the present study. In addition, Wang *et al*. (2020) conducted

Table 6 Comparison between the similar studies and the present research

	Wang *et al*. (2020)	Du *et al*. (2020)	This study
Material	Rock-like sample.	Sandstone.	Sandstone.
Fissure	Constant.	Different rock bridge parameters and constant fissure inclination.	Different fissure inclination.
Strength properties	Focused on the weakening of water pressure on strength properties.	Focused on the influence of rock bridge parameters on strength properties.	Compared the influence of fissure inclination, confining pressure, and water pressure on mechanical properties.
Crack behavior	Investigated only the effect of water pressure on failure patterns.	Compared crack coalescence patterns between the two fissures at different rock bridge parameters.	Discussed the synergistic effect of fissure inclination, confining pressure, and water pressure on crack behaviors. The emphasis is on the types, length, and numbers of cracks.
Inner failure analysis	None.	Qualitatively analyzed the inner failure behaviors based on CT images.	Changed CT images to binarized pictures using MATLAB software; quantitatively analyzed the inner crack area.
Permeability	Studied only the permeability evolution with volumetric strain of pre-cracked samples.	Discussed only the permeability behaviors of double-fissure samples.	Compared the permeability behaviors of intact samples and single-fissure samples.

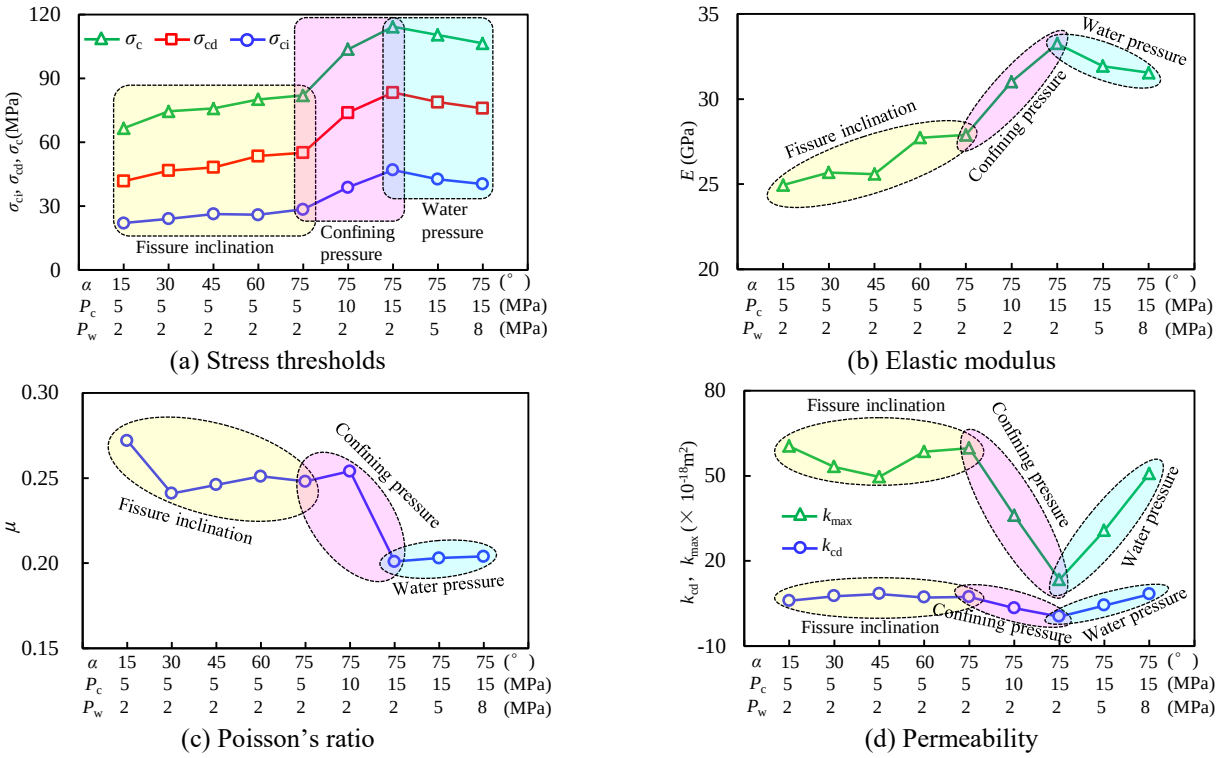

Fig. 18 Effect of α, P_c, and P_w on mechanical properties and permeability

hydro-mechanical experiments to investigate the strength and permeability behaviors of rock-like samples with four joints. Although rock-like materials and real rock materials have common characteristics for hydro-mechanical behaviors, there are also some differences between them caused by the material properties. Therefore, in our recent study (Du *et al*. 2020) and the present study, we performed many experiments by using sandstone to investigate the strength characteristics, fracture behaviors and permeability evolutions of pre-cracked real rocks. The differences between these similar studies (Wang *et al*. 2020, Du *et al*. 2020) and the present study are summarized in Table 6.

6.2 Summary of the effects of fissure inclination, confining pressure, and water pressure on hydro-mechanical behaviors of single-fissure samples

To compare the effects of fissure inclination, confining pressure, and water pressure on hydro-mechanical behaviors of single-fissure samples, the stress thresholds, elastic modulus, Poisson's ratio, and permeability of single-fissure samples with different inclinations and the samples with a 75° inclination fissure under different confining pressures and water pressures were analyzed statistically, as shown in Fig. 18.

Fig. 18(a) shows that when the fissure inclination changes from 15° to 75°, σ_{ci}, σ_{cd}, and σ_c of single-fissure samples are diversified in the ranges of 22.01-28.44, 41.71~55.07, and 66.53-82.01 MPa, respectively. When the confining pressure increases from 5 MPa to 15 MPa, their σ_{ci}, σ_{cd}, and σ_c are diversified in the ranges of 28.44-47.02, 55.07-83.37, and 82.01-114.26 MPa, respectively. When the confining pressure increases from 2 MPa to 8 MPa, their σ_{ci}, σ_{cd}, and σ_c are changed in the ranges of 40.36-47.02, 75.94-83.37, and 106.42-114.26 MPa, respectively. Therefore, the influence of fissure inclination on stress thresholds in the failure process of single-fissure samples is smaller than the influence of confining pressure but greater than the influence of water pressure. Generally, the stress thresholds gradually increase with an increase in fissure inclination and confining pressure and decrease with an increase in water pressure. Fig. 18(b) shows that the influence of fissure inclination, water pressure, and confining pressure on the elastic modulus is similar to that on stress thresholds. From Fig. 18(c), the changing trend of Poisson's ratio with fissure inclination, confining pressure, and water pressure is roughly opposite to that of stress thresholds and elastic modulus. The confining pressure has the greatest effect on Poisson's ratio, followed by the fissure inclination, and the water pressure. Fig. 18(d) indicates that the effect of fissure inclination, confining pressure, and water pressure on permeability is similar to that on Poisson's ratio. Moreover, the permeability in the volumetric dilation stage (e.g., k_{max}) is more sensitive to the three impact factors than the permeability in the volumetric contraction stage (e.g., k_{cd}). Briefly speaking, for mechanical properties, the effect of the three factors from high to low is as follows: confining pressure, fissure inclination, and water pressure. Nevertheless, the impact of fissure inclination on permeability is smaller than that of confining pressure and water pressure.

7. Conclusions

This research performed a series of experiments on

single-fissure sandstone samples to systematically explore the influence of fissure inclination, confining pressure, and water pressure on hydro-mechanical coupling behaviors of single-fissure sandstone. Compared with previous studies, the major discoveries on the mechanical properties, fracture characteristics, and permeability behaviors of sandstone samples containing a single fissure can be summarized as follows:

• From the aspect of mechanical analysis, the largest reductions in σ_{ci}, σ_{cd}, and σ_c induced by the fissure are 41.9%, 35.8%, and 23.6%, respectively, and the corresponding fissure inclination is generally smaller than 45°. The stress threshold and elastic modulus of single-fissure sandstone increase with increasing fissure inclination and confining pressure but decrease with increasing water pressure. However, the corresponding relationship with Poisson's ratio is approximately opposite. Furthermore, the confining pressure has the greatest effect on these mechanical properties, followed by the fissure inclination and water pressure.

• The influence law of confining pressure and water pressure on fracture behavior will change with the fissure inclination. At a lower fissure inclination, the confining pressure may change the type of the main cracks, and the water pressure increases the number of anti-wing cracks and the length of wing cracks and branch cracks. However, the fracture behaviors of samples with a higher fissure inclination are only slightly affected by the confining pressure and water pressure.

• Based on the CT images, the effect of fissure inclination on the internal crack area is reduced with the propagation from the fissure tips to the ends of samples. Unlike the wing and anti-wing cracks, the branch cracks are generally generated near the surface of the samples and do not penetrate the horizontal cross-sections.

• The fissure inclination mainly affects the value of the permeability but not affect the trend. Compared to intact samples, k_{cd} and k_{max} of single-fissure samples increase by at most 3.7×10^{-18} and 21.0×10^{-18} m^2 under the same condition, respectively. Furthermore, the changes in k_{max} induced by fissure inclination are more remarkable than those in k_{cd}, especially under a lower confining pressure or a higher water pressure. In addition, the impact of the pre-existing fissure on permeability is smaller than that of confining pressure and water pressure.

Acknowledgments

The research described in this paper was financially supported by the National Natural Science Foundation of China (NO. 41772299 and 51279096).

References

Alam, A.K.M.B., Niioka, M., Fujii, Y., Fukuda, D. and Kodama, J. (2014), "Effects of confining pressure on the permeability of three rock types under compression", *Int. J. Rock Mech. Min. Sci.*, **65**, 49-61. https://doi.org/10.1016/j.ijrmms.2013.11.006.

Asadizadeh, M., Hossaini, M.F., Moosavi, M., Masoumi, H. and Ranjith, P.G. (2019), "Mechanical characterisation of jointed rock-like material with non-persistent rough joints subjected to uniaxial compression", *Eng. Geol.*, **260**, 105224. https://doi.org/10.1016/j.enggeo.2019.105224.

Bastola, S. and Cai, M. (2019), "Investigation of mechanical properties and crack propagation in pre-cracked marbles using lattice-spring-based synthetic rock mass (LS-SRM) modeling approach", *Comput. Geotech.*, **110**, 28-43. https://doi.org/10.1016/j.compgeo.2019.02.009.

Bewick, R.P., Kaiser, P.K. and Amann, F. (2019), "Strength of massive to moderately jointed hard rock masses", *J. Rock Mech. Geotech. Eng.*, **11**(3), 562-575. https://doi.org/10.1016/j.jrmge.2018.10.003.

Bruning, T., Karakus, M., Nguyen, G.D. and Goodchild, D. (2018), "Experimental study on the damage evolution of brittle rock under triaxial confinement with full circumferential strain control", *Rock Mech. Rock Eng.*, **51**(11), 3321-3341. https://doi.org/10.1007/s00603-018-1537-7.

Chen, M., Yang, S.Q., Ranjith, P.G., Yang, W.D., Yin, P.F., Zhang, Y.C. and Zhang, Q.Y. (2019), "Fracture processes of rock-like specimens containing nonpersistent fissures under uniaxial compression", *Energies* **12**(1), 79. https://doi.org/10.3390/en12010079.

Chen, X., Yu, J., Tang, C.A., Li, H. and Wang, S.Y. (2017a), "Experimental and numerical investigation of permeability evolution with damage of sandstone under triaxial compression", *Rock Mech. Rock Eng.* **50**(6), 1529-1549. https://doi.org/10.1007/s00603-017-1169-3.

Chen, S.W., Yang, C.H. and Wang, G.B. (2017b), "Evolution of thermal damage and permeability of Beishan granite", *Appl. Therm. Eng.*, **110**, 1533-1542. https://doi.org/10.1016/j.applthermaleng.2016.09.075.

Crider, J.G. (2015), "The initiation of brittle faults in crystalline rock", *J. Struct. Geol.*, **77**, 159-174. https://doi.org/10.1016/j.jsg.2015.05.001.

Davy, C.A., Skoczylas, F., Barnichon, J.D. and Lebon P. (2007), "Permeability of macro-cracked argillite under confinement: Gas and water testing", *Phys. Chem. Earth.,* **32**(8-14), 66-680. https://doi.org/10.1016/j.pce.2006.02.055.

Du, Y.T., Li, T.C., Li, W.T., Ren, Y.D., Wang, G. and He, P. (2020), "Experimental study of mechanical and permeability behaviors during the failure of sandstone containing two preexisting fissures under triaxial compression", *Rock Mech. Rock Eng.*, **53**(8), 3673-3697. https://doi.org/10.1007/s00603-020-02119-x.

Duriez, J., Scholtes, L. and Donze, F.V. (2016), "Micromechanics of wing crack propagation for different flaw properties", *Eng. Fract. Mech.*, **153**, 378-398. https://doi.org/10.1016/j.engfracmech.2015.12.034.

Fu, J.W., Zhang, X.Z., Zhu, W.S., Chen, K. and Guan, J.F. (2017), "Simulating progressive failure in brittle jointed rock masses using a modified elastic-brittle model and the application", *Eng. Fract. Mech.*, **178**, 212-230. https://doi.org/10.1016/j.engfracmech.2017.04.037.

Heiland, J. (2003), "Permeability of triaxially compressed sandstone: influence of deformation and strain-rate on permeability", *Pure Appl. Geophys.*, **160**(5-6), 889-908. https://doi.org/10.1007/PL00012571.

Hu, J., Li, S.C., Liu, H.L., Li, L.P., Shi, S.S. and Qin, C.S. (2020), "New modified model for estimating the peak shear strength of rock mass containing nonconsecutive joint based on a simulated experiment", *Int. J. Geomech.*, **20**(7), 1-10. https://doi.org/10.1061/(ASCE)GM.1943-5622.0001732.

Huang, C.C., Yang, W.D., Duan, K., Fang, L.D., Wang, L. and Bo, C.J. (2019), "Mechanical behaviors of the brittle rock-like specimens with multi-non-persistent joints under uniaxial compression", *Constr. Build. Mater.*, **220**, 426-443. https://doi.org/10.1016/j.conbuildmat.2019.05.159.

Huang, D., Gu, D.M., Yang, C., Huang, R.Q. and Fu, G.Y. (2016a), "Investigation on mechanical behaviors of sandstone with two preexisting flaws under triaxial compression", *Rock Mech. Rock Eng.*, **49**, 375-399. https://doi.org/10.1007/s00603-015-0757-3.

Huang, Y.H., Yang S.Q. and Zhao, J. (2016b) "Three-dimensional numerical simulation on triaxial failure mechanical behavior of rock-like specimen containing two unparallel fissures", *Rock Mech. Rock Eng.*, **49**(12), 4711-4729. https://doi.org/10.1007/s00603-016-1081-2.

Jin, J., Cao, P., Chen, Y., Pu, C.Z., Mao, D.W. and Fan, X. (2017), "Influence of single flaw on the failure process and energy mechanics of rock-like material", *Comput. Geotech.*, **86**, 150-162. https://doi.org/10.1016/j.compgeo.2017.01.011.

Lee, H. and Jeon, S. (2011), "An experimental and numerical study of fracture coalescence in pre-cracked specimens under uniaxial compression", *Int. J. Solids Struct.*, **48**(6), 979-999. https://doi.org/10.1016/j.ijsolstr.2010.12.001.

Lee, J. and Hong, J.W. (2018), "Crack initiation and fragmentation processes in pre-cracked rock-like materials", *Geomech. Eng.*, **15**(5), 1047-1059. https://doi.org/10.12989/gae.2018.15.5.1047.

Li, T.C., Lyu, L.X., Zhang, S.L. and Sun, J.C. (2015), "Development and application of a statistical constitutive model of damaged rock affected by the load-bearing capacity of damaged elements", *J. Zhejiang Univ. Sci. A*, **16**(8), 644-655. https://doi.org/10.1631/jzus.A1500034.

Liu, L.W., Li, H.B., Li, X.F. and Wu, R.J. (2020), "Full-field strain evolution and characteristic stress levels of rocks containing a single pre-existing flaw under uniaxial compression", *B. Eng. Geol. Environ.*, **79**(6), 3145-3161. https://doi.org/10.1007/s10064-020-01764-4.

Manouchehrian, A., Sharifzadeh, M., Marji, M.F. and Gholamnejad, J. (2014), "A bonded particle model for analysis of the flaw orientation effect on crack propagation mechanism in brittle materials under compression", *Arch. Civ. Mech. Eng.*, **14**(1), 40-52. https://doi.org/10.1016/j.acme.2013.05.008.

Martin, C.D. and Chandler, N.A. (1994), "The progressive fracture of lac du bonnet granite", *Int. J. Rock Mech. Min. Sci.*, **31**(6), 643-659. https://doi.org/10.1016/0148-9062(94)90005-1.

Maruvanchery, V. and Kim, E. (2018), "Effects of water on rock fracture properties: Studies of mode I fracture toughness, crack propagation velocity, and consumed energy in calcite-cemented sandstone", *Geomech. Eng.*, **17**(1), 57-67. https://doi.org/10.12989/gae.2019.17.1.057.

Mondal, S., Olsen-Kettle, L. and Gross, L. (2019), "Simulating damage evolution and fracture propagation in sandstone containing a preexisting 3-D surface flaw under uniaxial compression", *Int. J. Numer. Anal. Met. Geomech.*, **43**(7), 1448-1466. https://doi.org/10.1002/nag.2908.

Morgan, S.P., Johnson, C.A. and Einstein, H.H. (2013), "Cracking processes in barre granite: Fracture process zones and crack coalescence", *Int. J. Fract.*, **180**(2), 177-204. https://doi.org/10.1007/s10704-013-9810-y.

Naderloo, M., Moosavi, M. and Ahmadi, M. (2019), "Using acoustic emission technique to monitor damage progress around joints in brittle materials", *Theor. Appl. Fract. Mec.*, **104**, 102368. https://doi.org/10.1016/j.tafmec.2019.102368.

Pakzad, R., Wang, S.Y. and Sloan, S. (2018), "Numerical study of the failure response and fracture propagation for rock specimens with preexisting flaws under compression", *Int. J. Geomech.*, **18**(7), 04018070. https://doi.org/10.1061/(ASCE)GM.1943-5622.0001172.

Park, C.H. and Bobet, A. (2010), "A crack initiation, propagation and coalescence from frictional flaws in uniaxial compression", *Eng. Fract. Mech.*, **77**(14), 2727-2748. https://doi.org/10.1016/j.engfracmech.2010.06.027.

Son, M. and Adedokun, S. (2016), "Effect of joint inclination angles on the earth pressure against the support system in a jointed rock mass", *KSCE J. Civ. Eng.*, **20**(4), 1259-1266. https://doi.org/10.1007/s12205-015-0487-9.

Tian, W.L. and Yang, S.Q. (2017), "Experimental and numerical study on the fracture coalescence behavior of rock-like materials containing two non-coplanar filled fissures under uniaxial compression", *Geomech. Eng.*, **12**(3), 541-560. https://doi.org/10.12989/gae.2017.12.3.541.

Wang, X.T., Li, S.C., Xu, Z.H., Li, X.Z., Lin, P. and Lin, C.J. (2019), "An interval risk assessment method and management of water inflow and inrush in course of karst tunnel excavation", *Tunn. Undergr. Sp. Tech.*, **92**, 103033. https://doi.org/10.1016/j.tust.2019.103033.

Wang, H.L., Zhao, K., Qu, X., Xu, J.R. and Cai, M. (2020), "Hydro-mechanical properties of rock-like specimens with pre-existing intermittent joints", *Eur. J. Environ. Civ. Eng.* https://doi.org/10.1080/19648189.2020.1763853.

Wong, L.N.Y. and Xiong, Q.Q. (2018), "A method for multiscale interpretation of fracture processes in carrara marble specimen containing a single flaw under uniaxial compression", *J. Geophys. Res-Sol. Ea.*, **123**(8), 6459-6490. https://doi.org/10.1029/2018JB015447.

Wu, J.Y., Feng, M.M., Han, G.S., Yao, B.Y. and Ni, X.Y. (2019), "Loading rate and confining pressure effect on dilatancy, acoustic emission, and failure characteristics of fissured rock with two pre-existing flaws", *Comptes Rendus Mecanique,* **347**(1), 62-89. https://doi.org/10.1016/j.crme.2018.10.002.

Xiao, W.J., Zhang, D.M. and Wang, X.J. (2020), "Experimental study on progressive failure process and permeability characteristics of red sandstone under seepage pressure", *Eng. Geol.*, **265**, 105406. https://doi.org/10.1016/j.enggeo.2019.105406.

Xu, J. and Li, Z.X. (2019), "Crack propagation and coalescence of step-path failure in rocks", *Rock Mech. Rock Eng.*, **52**(4), 965-979. https://doi.org/10.1007/s00603-018-1661-4.

Yang, S.Q., Ranjith, P.G., Huang, Y.H., Yin, P.F., Jing, H.W., Gui, Y.L. and Yu, Q.L (2015), "Experimental investigation on mechanical damage characteristics of sandstone under triaxial cyclic loading", *Geophys. J. Int.*, **201**, 662-682. https://doi.org/10.1093/gji/ggv023.

Yu, J., Yao, W., Duan, K., Liu, X.Y. and Zhu, Y.L. (2020), "Experimental study and discrete element method modeling of compression and permeability behaviors of weakly anisotropic sandstones", *Int. J. Rock Mech. Min. Sci.*, **134**, 104437. https://doi.org/10.1016/j.ijrmms.2020.104437.

Zeng, W., Yang, S.Q., Tian, W.L. and Wen, K. (2018), "Numerical investigation on permeability evolution behavior of rock by an improved flow-coupling algorithm in particle flow code", *J. Cent. South Univ.*, **25**(6), 1367-1385. https://doi.org/10.1007/s11771-018-3833-5.

Zhao, C., Niu, J.L., Zhang, Q.Z., Zhao, C.F. and Zhou, Y.M. (2019), "Failure characteristics of rock-like materials with single flaws under uniaxial compression", *B. Eng. Geol. Environ.*, **78**(1), 593-603. https://doi.org/10.1007/s10064-018-1379-2.

CC